RSC Advances

ROYAL SOCIETY OF CHEMISTRY

www.rsc.org/advances

RSC Advances

ARTICLE

Synergistic lithium storage of multi-component $Co_2SnO_4/Co_3O_4/Al_2O_3/C$ composite from single-source precursor

Received 00th January 20xx,
Accepted 00th January 20xx

DOI: 10.1039/x0xx00000x

www.rsc.org/

Bibo Wu, Shilin Zhang, Feng Yao, Fazhi Zhang, Sailong Xu*

Endowing multi-component anode nanomaterials for lithium-ion batteries (LIBs) with integrated features synergistically enhancing electrochemical performances is challenging via a simple preparation method. We herein describe an easy approach to prepare multi-component $Co_2SnO_4/Co_3O_4/Al_2O_3/C$ composite as anode nanomaterial for LIBs derived from a laurate anion-intercalated CoAlSn-layered double hydroxide (CoAlSn-LDH) single-source precursor. The resultant $Co_2SnO_4/Co_3O_4/Al_2O_3/C$ electrode delivers a highly enhanced reversiable capacity of 1170 mA h g^{-1} at 100 mA g^{-1} upon 100 cycles, compared with the bi-active composites designed without Al_2O_3 or carbon ($Co_2SnO_4/Co_3O_4/C$, $Co_2SnO_4/Co_3O_4/Al_2O_3$, and Co_2SnO_4/Co_3O_4) which are easily derived through the same protocol by chosing the LDH precursors without Al cation or surfactant intercalation. The distinctly different cycling stability and rate capability of $Co_2SnO_4/Co_3O_4/Al_2O_3/C$ among the designed different composite electrodes, justifies that the high enhancement could benefit from the synergistic features: combined conversion and alloying reactions of bi-active Co_2SnO_4/Co_3O_4 during cycling, buffering role of non-active Al_2O_3 and carbon, and improved conductivity of the self-generated carbon matrix. The LDH precursor-based approach may initial designing and preparing various multi-component transition metal oxide composite nanomaterials for synergistic lithium storage.

1 Introduction

Rechargeable lithium-ion batteries (LIBs) have been the dominant power source for portable electronic devices and promising as the critical candidate for the next-generation electric vehicles.[1-3] Rapidly widening market applications of LIBs increasingly inspire development of electrode nanomaterials with improved capacity, long cycle life, high power density and energy density. Much effort has been devoted to introducing additional active component to improve transitional metal oxides (TMOs)-based nanostructures[4,5] as anode nanomaterials for LIBs, thereby alleviating the common problems of large voltage hysteresis and irreversible capacity. These studies rang from single ternary TMOs (such as hollow porous $CoFe_2O_4$ nanocube,[6] Co_2SnO_4/graphene oxide,[7] porous hierarchical tremella-like $NiMn_2O_4/C$[8]), to composite ternary TMOs[9-11] ($CoO/CoFe_2O_4$, Co_3O_4/Co_2MnO_4, and Mn_3O_4/Zn_2SnO_4). These nanomaterials were able to deliver enhanced reversible capacities owing to the multi-component synergism. However, most TMOs still suffer from structural variation resulted from aggregation of nanoparticles into large particles during cycling, and also from fast capacity decay thanks to poor conductivity,[12,13] especially for the exquisitely designed hierarchical micro/nanostructures.

Introduction of non-active components (such as Al_2O_3 or ZnO) into TMO composites is also crucial to enhance cycling stability and rate performance. This design strategy has been successfully applied to electrode nanomaterials for LIBs, in which non-active components (such as Al_2O_3 or ZnO) can act as buffering medium to effectively alleviate volume changes of the actives during the cycles and also to prevent aggregation of electrochemically active nanoparticles, thereby maintaining the structural integrity of the electrode nanomaterials.[14,15] ZnO-containing $ZnO/ZnFe_2O_4$ nanocube was found to deliver a high capacity of 800 mA h g^{-1} at 1000 mA g^{-1} after 200 cycles, though derived by using toxic $K_3Fe(CN)_6$ with hypertoxic product upon exposure to acidic or heated conditions.[16] Also, $ZnMn_2O_4/ZnO/C$ nanohybrid exhibited a reversible capacity of 520 mA h g^{-1} at 800 mA g^{-1} after 100 cycles, which was synthetized initially by ball-milling mixed precursors of $ZnMnO_3$ and acetylene black in absolute alcohol for 5 h, and subsequently by calcination at 600 °C under an argon atmosphere for 5 h.[17] Similarly, Al_2O_3-coated Fe_3O_4/reduced graphene oxide electrode achieved a reversible capacity of 717 mA h g^{-1} after 200 cycles at a current density of 1/2 C, of which the thickness of the Al_2O_3 coating was elaborately controlled within few nanometers using atomic layer deposition (ALD) technique.[18] The introduction of the non-active composites was, however, obtained typically using expensive or energy-consumed equipmentss or complicated procedures. It is thus of great importance to develop carbon supported active/non-active TMO composites by using simple,

State Key Laboratory of Chemical Resource Engineering, Beijing University of Chemical Technology, Beijing 100029, China; E-mail: xusl@mail.buct.edu.cn.
Electronic Supplementary Information (ESI) available: XRD, TEM, XPS, and charge-discharge profiles. See DOI: 10.1039/x0xx00000x

economic and also scalable methods.

Layered double hydroxides (LDHs) are one type of anionic lamellar potential precursor materials. LDHs are typically described by the general formula $[M^{II}_{1-x}M^{III}_{x}(OH)_2]^{x+}(A^{n-})_{x/n}\cdot yH_2O$, where M^{II} and M^{III} are type-and-ratio-tunable cations occupying the octahedral holes in a brucite $Mg(OH)_2$-like layer, and A^{n-} is a type-tunable anion intercalated between the hydrated interlayer galleries. Thermal treatment of LDH precursors has been demonstrated to be an alternative method for the fabrication of various mixed metal oxide composites with well-dispersed multiple components.[19-22] We have recently demonstrated that C-Ni@NiO/Al_2O_3, derived from NiAl-LDH/glucose mixture[23], was able to deliver a stable charge capacity of 551 mA h g^{-1} upon 80 cycles at 100 mA g^{-1}, however, with a low reversible capacity and the hypothesis of the conductive carbon and buffering Al_2O_3 to improve the cycling stability and rate capability.

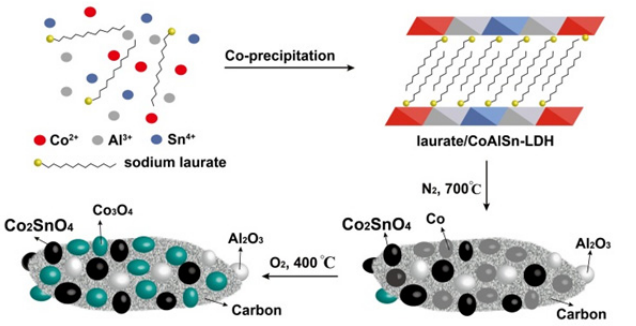

Fig. 1 Schematic illustration of formation of $Co_2SnO_4/Co_3O_4/Al_2O_3/C$ composite.

In this study, we describe a multi-component $Co_2SnO_4/Co_3O_4/Al_2O_3/C$ composite derived from a single-source precursor of laurate anion (LA^-) -intercalated ternary CoAlSn-LDH (CoAlSn-LA^--LDH) via calcination and further oxidation procedure (Fig. 1). The ternary CoAlSn-LDH host was chosen due to considering utilization of combined conversion and alloying reactions of bi-active Co_2SnO_4/Co_3O_4 during cycling to improve electrochemical capacity.[24,25,26] Electrochemical evaluation shows that the resultant $Co_2SnO_4/Co_3O_4/Al_2O_3/C$ composite indeed exhibits highly enhanced electrochemical performances, in comparison with the different bi-active composites involving Co_2SnO_4/Co_3O_4, $Co_2SnO_4/Co_3O_4/C$, and $Co_2SnO_4/Co_3O_4/Al_2O_3$. The distinctly different cycling stability and rate capability of $Co_2SnO_4/Co_3O_4/Al_2O_3/C$ among the designed different composite electrodes, justifies the possibilities of benefiting the high enhancements, which is easily achieved through the same protocol by choosing the LDH precursors without Al cation or surfactant intercalation.

2 Experimental Sections

2.1. Preparation

The CoAlSn-LA^--LDH precursor was synthesized via a conventional co-precipitation method. In brief, a mixture of $Co(NO_3)_2\cdot 6H_2O$ (0.03 mol), $Al(NO_3)_3\cdot 9H_2O$ (0.005 mol), and $SnCl_4\cdot 4H_2O$ (0.005 mol) were dissolved in 100 mL distilled water, and then titrated by adding a solution of 100 mL NaOH (0.05 mol) and sodium laurate (0.015 mol) with stirring under N_2 atmosphere at room temperature until pH = 10.5 ± 0.1, followed by aging at 120 °C for 24 h. Afterwards, the precipitates obtained were centrifuged, washed with distilled water, and dried at 60 °C in vacuum oven overnight.

$Co_2SnO_4/Co_3O_4/Al_2O_3/C$ was obtained by calcination of the precursor in a fused quartz tube mounted in a programmable tube furnace at 700 °C for 200 min under N_2 atmosphere with a temperature ramping rate of 2 °C /min. Then a further calcination was employed in air at 400 °C for 120 min, followed by subsequent cooling to ambient temperature.

For comparison, $Co_2SnO_4/Co_3O_4/Al_2O_3$ was prepared using the same protocol from the CoAlSn-LDH without the intercalation of laurate anion, and $Co_2SnO_4/Co_3O_4/C$ and Co_2SnO_4/Co_3O_4 were obtained from CoSn-LDH with and without the intercalation of laurate anion, respectively.

2.2 Characterization

Powder XRD measurements were performed on a Rigaku XRD 6000 diffractometer, using Kα (40 kV, 30 mA, λ = 0.1542 nm) in the 2θ range from 3 to 70°. Morphology and chemical composition of the samples were investigated by using scanning electron microscope (SEM, ZEISS Supra 55). The accelerating voltage was 20 kV. Transmission electron microscopy (TEM, JEM JEOL 2100) was used to visualize the morphologies, sizes and structures of the products. High-resolution transmission electron microscopy (HRTEM) images were recorded on JEOL JEM-2100 microscope. High-angle annular dark field scanning transmission electron microscopy (HAADF-STEM) imaging and EDX mapping was performed on Tecnai G2 F30 S-TWIN equipped with energy dispersive X-ray (EDX). Room-temperature FTIR spectra were recorded in the range 400–4000 cm^{-1} with a resolution of 2 cm^{-1} on a Bruker Vector-22 Fourier transform spectrometer using the KBr pellet technique (1 mg of sample in 100 mg of KBr). Raman spectroscopy was recorded on a confocal Raman spectrometer (Renishaw RM2000) with a 532 nm excitation laser (laser spot size of 0.5 μm) operated at a low power level (~2 mW). Samples were drop-cast onto a silicon substrate for measurements. X-ray photoelectron spectroscopy (XPS) (Thermo VG Scientific) was recorded under high vacuum on samples dried onto silicon wafers using Al Kα 1486.6 eV radiation at 400 W (15 kV).

2.3 Electrochemical measurements

Electrochemical measurements were performed with 2032 coin cells assembled in an Ar-filled glove box. Active material, Pketjen black, and poly (vinyl difluoride) (PVDF) with a 70: 20: 10 weight ratio were mixed and pasted on a Cu foil, thereby preparing working electrodes. The loading mass of composite material is about 10 mg cm^{-2}. Lithium foil was used as the counter electrode, and a glass fiber (GF/D, from Whatman) as a separator. The used electrolyte consisted of a solution of 1M $LiPF_6$ salt in ethylene carbonate (EC)/dimethyl carbonate (DMC)/ (1:1 by wt. %) (obtained from Tianjing Jinniu Power Sources Material Co. Ltd.). Galvanostatic cycling and the charge-discharge profile of the assembled cells was carried out using LAND CT2001A battery tester in the voltage range from 0.01 to 3.0 V (*vs.* Li^+/Li). Cyclic voltammogram (CV) was measured on an electrochemistry workstation (CHI 660E) at a scan rate of 0.1 mV s^{-1} in the voltage range of 0–3.0V (*vs.* Li^+/Li). EIS

measurement was performed over the frequency range between 100 KHz and 0.1 Hz at open circuit potential using on a Parstat 2273 advanced electrochemical system.

3 Results and Discussion

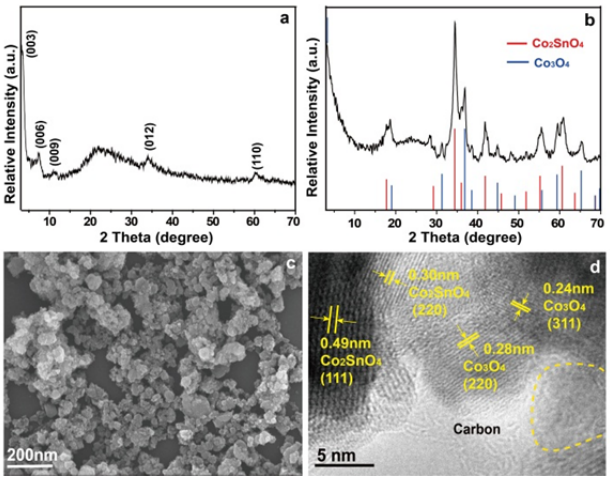

Fig. 2 (a) XRD patterns of CoAlSn-LA^{-}-LDH precursor, (b) XRD patterns, as well as (c) SEM and (d) HRTEM images of $Co_2SnO_4/Co_3O_4/Al_2O_3/C$ composite.

The CoAlSn-LA^{-}-LDH precursor was prepared by using a conventional co-precipitation method. XRD results show that a shift of the (003) basal peak was clearly visible for the resulting precursor at an angle $2\theta < 10^{\circ}$ (Fig. 2a), which is lower than that ($2\theta = 11.6^{\circ}$) of the pristine CoAlSn-CO_3^{2-}-LDH (Fig. S1a†). This pronounced shift strongly suggests the intercalation of the surfactant into the interlayer galleries.[27] After the completion of calcining the precursor, the obtained product shows the XRD characteristics of Co_2SnO_4 and Co_3O_4 (Fig. 2b). The diffraction peaks observed at 2θ values of 17.8, 29.2, 34.4, 36, 42, 45.7, 51.8, 55.2, 60.6 and 63.7° can be well indexed to (111), (220), (311), (222), (400), (331), (422), (511), (440), and (531) planes of Co_2SnO_4 (JCPDS 29-0514), respectively, and the other diffraction peaks to Co_3O_4 (JCPDS 43-1003). A halo was discerned with an angular range from 20° to 30°, attributable to the amorphous carbonaceous material formed upon the carbonization process. Additionally, no characteristic peak was visible for Al_2O_3, indicative of the amorphous Al_2O_3 phase. This amorphous feature is indeed consistent with the previous studies of our and others' laboratories concerning Al_2O_3-containing composites derived from surfactants intercalated LDHs.[23,28,29] For comparison, the other three bi-active Co_2SnO_4/Co_3O_4 composites were obtained, easily by varying cation type of LDH precursors. Comparison of XRD patterns of all the bi-active composites, clearly shows the consistence of bi-active-component basal reflection peaks (as shown in Fig. 2b and Fig. S1b†), thus strongly suggestive of the feasibility and good reproducibility of the preparation method.

Surface morphology was observed for the $Co_2SnO_4/Co_3O_4/Al_2O_3/C$ composite using SEM. Fig. 2c displays a particle-like morphology of the composite. The small dimensional sizes can be assigned to the confinement, which is from both the net trap effect of both Al_2O_3 and the carbon formed via carbonization during the high-temperature calcination.[23] TEM visualization confirms the formation of carbon-supported nanoparticles (Fig. S2†). Such a similar size distribution was also observed for the $Co_2SnO_4/Co_3O_4/C$ composite with carbon (Fig. S3a†), which was derived from the CoSn-LA^{-}-LDH precursor without Al cation. High-resolution TEM of the $Co_2SnO_4/Co_3O_4/Al_2O_3/C$ composite further justifies the co-existence of carbon-supported bi- and non-active $Co_2SnO_4/Co_3O_4/Al_2O_3$ (Fig. 2d). Two types of highly crystalline regions were resolved, with the d-spacing values of 0.49 and 0.3 nm corresponding to the (111) and (220) planes of cubic Co_2SnO_4, and also with those of 0.24 and 0.28 nm corresponding to (311) and (220) planes of cubic Co_3O_4. The involved planes are well consistent with the above-mentioned XRD patterns of the $Co_2SnO_4/Co_3O_4/Al_2O_3/C$ composite. One domain with curved and bent graphene-like sheets can be ascribed to carbon. In addition, note that the bi-active composites without carbon, i.e., $Co_2SnO_4/Co_3O_4/Al_2O_3$ and Co_2SnO_4/Co_3O_4, both were found to be more homogenous in dimensional size distribution, but larger in dimensional size and crystalline size, as shown in SEM (Fig. S3b-c†) and TEM images (Fig. S3e-f†), when compared with both bi-active composites with carbon (Fig. 2c-d, Fig. S3a and Fig. 3d†). A dotted-line-circle marked domain could be identified as amorphous Al_2O_3 or carbon, owing to the limited instrumental resolution (Fig. 2d). We additionally carried out HAADF-STEM imaging and EDX mapping on the $Co_2SnO_4/Co_3O_4/Al_2O_3/C$ composite. The resulting HAADF-STEM/EDX observations (Fig. S4†) show the nanoparticle-like morphology of the composite. The majority elements Co and O, as well as the minority elements of Al and Sn, are well dispersed within the composite nanoparticles, indeed in agreement with the molar ratios of the LDH precursor.

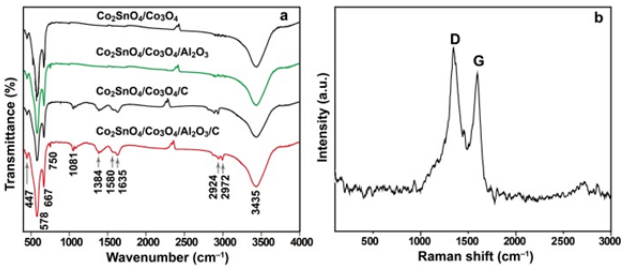

Fig. 3 (a) FT-IR spectra of $Co_2SnO_4/Co_3O_4/Al_2O_3/C$, Co_2SnO_4/Co_3O_4, $Co_2SnO_4/Co_3O_4/Al_2O_3$, and $Co_2SnO_4/Co_3O_4/C$ composites. (b) Raman spectrum of the $Co_2SnO_4/Co_3O_4/Al_2O_3/C$ composite.

FT-IR spectrum was recorded for $Co_2SnO_4/Co_3O_4/Al_2O_3/C$ and the other three composites. Fig. 3a depicts that all the composites exhibit similar adsorption bands of each component contained. Two absorption peaks were identified at 447 and 578 cm^{-1}, corresponding to the stretching vibration of Co^{2+}-O and Co^{3+}-O bonds, respectively. The absorption band at 667 cm^{-1} can be assigned to the asymmetric vibration of Sn-O-Sn bond, and the one at 750 cm^{-1} to the stretching vibration of Al-O band.[30,31] The broad and strong absorption band was visible around 3435 cm^{-1}, ascribed to the symmetric stretching vibration of -OH group owing to the presence of adsorbed moisture.[26] In the case of the composites with carbon, two absorption peaks were resolved at 1580 and 1635 cm^{-1}, ascribed to the stretching vibration of C=C and stretching vibration of C=O

separately, and the ones at 1384 and 1081 cm^{-1} to the stretching vibration absorption of C-O bond. Absorption peaks at 2924 and 2972 cm^{-1} confirm the symmetric and asymmetric stretching vibrations of C-H bond, respectively.[32,33] These results elucidate the formation of carbon, which is converted from the long alkyl chains of laurate anions during the thermal treatment. Raman analysis further manifests the nature of the carbon support of $Co_2SnO_4/Co_3O_4/Al_2O_3/C$ (Fig. 3b). Two broad peaks at 1340 (D-band) and 1586 cm^{-1} (G-band) were clearly visible, corresponding to the disorder induced along the c-axis of graphitic carbonaceous material and to the vibration of sp^2 hybridized carbon atoms in graphitic carbon,[34] respectively. The calculated I_D/I_G ratio was 1.15, indicative of the highly disordered feature of the carbon matrix.[35]

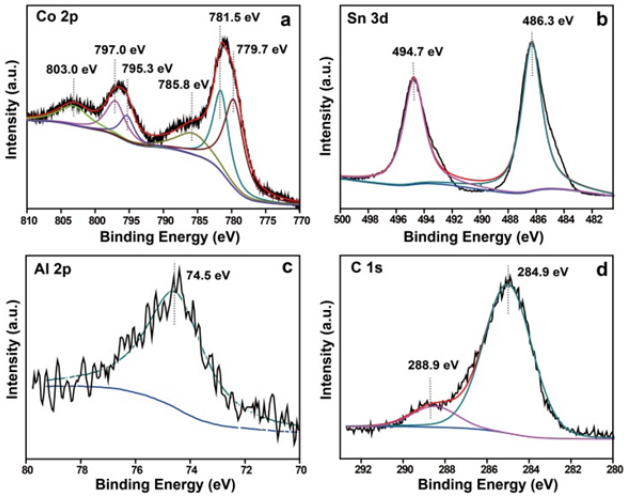

Fig. 4 XPS spectra of $Co_2SnO_4/Co_3O_4/Al_2O_3/C$ composite for (a) Co 2p, (b) Sn 3d, (c) Al 2p and (d) C 1s.

Chemical state was characterized for the $Co_2SnO_4/Co_3O_4/Al_2O_3/C$ composite by XPS technique (Fig. 4). The high-resolution of Co 2p spectrum shows two obvious spin orbit doublet peaks centred at 781.5 and 797.0 eV, accompanied with two prominent shake-up satellite peaks at 785.8 and 803.0 eV, respectively. These four peaks can be ascribed to Co $2p_{3/2}$ and Co $2p_{1/2}$ orbits,[36,37] obviously verifying the presence of the Co^{2+}. Another two major peaks centred at 779.7 and 795.3 eV can be attributable to Co $2p_{3/2}$ and Co $2p_{1/2}$ of the Co_3O_4 phase, respectively.[38] Fig. 4b displays that the Sn 3d spectrum can be fitted by two strong energy bands centred at 486.3 and 494.7 eV, which are ascribed to the $3d_{5/2}$ and $3d_{3/2}$ orbits, respectively.[36,37] In addition, Al 2p spectrum shows one major peak at 74.5 eV (Fig. 4c), indicative of the formation of amorphous Al_2O_3 phase.[23,39] Also, C 1s XPS spectrum could be fitted by two strong peaks at 284.9 and 288.9 eV (Fig. 4d), which can be ascribed to the presence of C-C and C-O of the supporting carbon matrix.[40] Comparison of Co 2p and Sn 3d spectra between these four composites (Fig. S5†) reveals that cobalt cations are present in the valent states of Co^{2+} and Co^{3+}, and tin cation is in the valent state of Sn^{4+}, again confirming the consistent reproducibility to prepare the bi-active Co_2SnO_4/Co_3O_4 composites through the protocol.

Furthermore, the contents of Co, Al and Sn of the nanomaterial were determined on the basis of the XPS data. A $Co_2SnO_4/Co_3O_4/Al_2O_3$ mass ratio was calculated to be 48.6: 44.5: 6.9. The molar ratio of Co/(Al+Sn) was thus determined to b 2.85, quite close to that (ca. 3.0) of the starting materials used. Result of element analysis gives rise to a 6.1 wt. % content of carbon. From various early studies,[23,28,29] the multiple components, including nanosized bi-active Co_2SnO_4/Co_3O_4, low-content non-active Al_2O_3, and self-generated conductive carbon, are expected to synergistically facilitate the reversible specific capacity and cycling stability of the $Co_2SnO_4/Co_3O_4/Al_2O_3/C$ nanocomposite when used as anode nanomaterials for LIBs.

Cyclic voltammetry (CV) curves were recorded for the $Co_2SnO_4/Co_3O_4/Al_2O_3/C$ electrode. Fig. 5a shows that a strong reduction peak was found at 0.55 V (*vs.* Li^+/Li) in the first cycle in

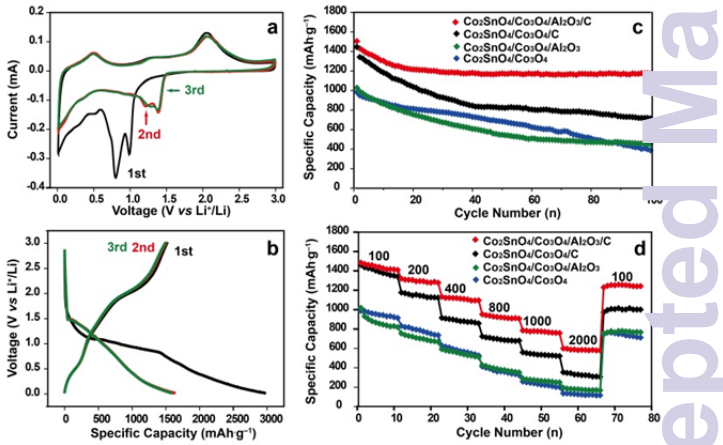

Fig. 5 (a) The first three cyclic voltammetry curves between 0–3.0 V at 0.1 mV s^{-1}, (b) the first three charge-discharge profiles at 100 mA g^{-1} of the $Co_2SnO_4/Co_3O_4/Al_2O_3/C$ composite, (c) cycling behaviour of charge capacity at a rate of 100 mA g^{-1}, and (d) rate capacity from 100, through 200, 400, 800, 1000, 2000, to 100 mA g^{-1} of $Co_2SnO_4/Co_3O_4/Al_2O_3/C$, Co_2SnO_4/Co_3O_4, $Co_2SnO_4/Co_3O_4/Al_2O_3$ and $Co_2SnO_4/Co_3O_4/C$ composites.

the cathodic process, attributable to the formation of solid electrolyte interface (SEI) and Li_2O, and the decomposition of Co_2SnO_4 and Co_3O_4,[24,41,42] as shown by the following Reactions 1 and 2. Another reduction peak was observed at 1.0 V (*vs.* Li^+/Li), corresponding to the formation of Li-Sn alloys, as accounted well by Reaction 3. In the anodic process, two broad oxidation peaks were clearly visible at 0.5 and 2.1 V, typically assigned to the de-alloying process (inverse response of Reaction 3) and the re-oxidation reaction of cobalt and tin atoms (as expressed by Reactions 4 and 5), respectively.[24] At the second and subsequent cycles, the cathodic peaks were found to shift remarkably to 1.2 V and 1.4 V, whereas no obvious shift was observed for the anodic process, as also reported in previous studies.[24,26,41] On the basis of the above CV curves, together with the storage mechanisms of Co_2SnO_4 and Co_3O_4 that have been widely reported previously,[7,24,25,42] a combined reaction mechanism involving intercalation and conversion reactions, may occur between Co_2SnO_4 and Co_3O_4 with Li^+. The electrochemical reactions for the $Co_2SnO_4/Co_3O_4/Al_2O_3/C$ composite could thus be summarized by the following reactions:

$$Co_2SnO_4 + 8Li^+ + 8e^- \rightarrow 2Co + Sn + 4Li_2O \quad (1)$$

$$Co_3O_4 + 8Li^+ + 8e^- \leftrightarrow 3Co + 4Li_2O \quad (2)$$

$$Sn + 4.4Li \leftrightarrow Li_{4.4}Sn \quad (3)$$

$$Sn + 2Li_2O \leftrightarrow SnO_2 + 4Li \quad (4)$$

$$Co + Li_2O \leftrightarrow CoO + 2Li \quad (5)$$

Galvanostatic discharge/charge test was performed for the $Co_2SnO_4/Co_3O_4/Al_2O_3/C$ electrode between 0.01–3 V at 100 mA g^{-1} (Fig. 5b). It is noteworthy that the initial capacity (1515 mA h g^{-1}) of $Co_2SnO_4/Co_3O_4/Al_2O_3/C$ electrode is slightly higher than that (1420 mA h g^{-1}) of the $Co_2SnO_4/Co_3O_4/C$ electrode. However, the theoretical capacity of the former with Al_2O_3 was calculated to be 935 mA h g^{-1}, slightly lower than that (1053 mA h g^{-1}) of the latter without Al_2O_3. This disagreement strongly suggests the enhancement in initial capacity of the $Co_2SnO_4/Co_3O_4/Al_2O_3/C$ electrode, which can be ascribed to the nanosized effect[43] of the $Co_2SnO_4/Co_3O_4/Al_2O_3/C$ composite. As observed above by TEM, the $Co_2SnO_4/Co_3O_4/Al_2O_3/C$ nanoparticles show a slightly smaller mean dimensional size (ca. 8.2 nm) than that (ca. 12.5 nm) of the $Co_2SnO_4/Co_3O_4/C$ nanoparticles, which can be ascribed to the confinements from the net trap effect[23] of non-active Al of the CoAlSn-LDH precursor, and also from the carbon formed. From a previous study, metal cations within the LDH layers have been demonstrated to adopt a fully ordered arrangement[44]. During thermal decomposition of the LDH precursors, the symbiotic non-active Al_2O_3 component serves a well-dispersed confining domain to prevent the growth and agglomeration of active Co_2SnO_4/Co_3O_4 nanoparticles. Therefore, the nanosized $Co_2SnO_4/Co_3O_4/Al_2O_3/C$ composite is able to exhibit the improved initial reversible capacity at the first cycling. In addition, a low initial Coulombic efficiency was determined to be 51.2%. The capacity loss can be generally attributed to the formation of SEI film during the first charge.[45] Although a close similarity in the former three discharge/charge profiles was found between the electrodes of $Co_2SnO_4/Co_3O_4/Al_2O_3/C$ and the other three composites (Fig. S6†), further comparison reveals a remarkable difference in cycling performance between the $Co_2SnO_4/Co_3O_4/Al_2O_3/C$ and other three electrodes. During 100 cycles, the Coulombic efficiencies of $Co_2SnO_4/Co_3O_4/Al_2O_3/C$ were found to retain stable (Fig. S7†). After the 100th cycling, the reversible charge capacity of $Co_2SnO_4/Co_3O_4/Al_2O_3/C$ is 1170 mA h g^{-1}, higher than the theoretical values of Co_2SnO_4 (1105 mA h g^{-1}) and Co_3O_4 (890 mA h g^{-1}). However, all the other three electrodes exhibit a rapid decay in reversible capacity during the cycling processes. The enhanced reversible capacity could be typically attributed to the synergistic effect of the above-mentioned multiphase reaction between bi-active Co_2SnO_4 and Co_3O_4, as observed for transition metal oxide composites.[11,24,26,46,47] Further comparison of reversible specific capacity was summarized in Table S1†, between our $Co_2SnO_4/Co_3O_4/Al_2O_3/C$ and the Co_2SnO_4- or Co_3O_4-based electrodes reported previously.[7,24,42,43,47-50] We found that the reversible charge capacity of our composite electrode may be comparable to those other electrodes when considering the approximate mass weights of the active materials used.

From various early studies[16-18,51-53], it well known that active component reacts with lithium, while non-active component acts as an electrochemically inert matrix and buffers the volume change during the charge/discharge cycle, thereby resulting in remarkable improvements in cycle life of the composite nanomaterials. To understand the role of non-active Al_2O_3, further comparison of cycling performance was employed between the composite electrodes with and without Al_2O_3. We can see that the $Co_2SnO_4/Co_3O_4/C$ electrode without Al_2O_3 was able to show a reversible capacity comparable to that of the $Co_2SnO_4/Co_3O_4/Al_2O_3/C$ electrode before the former 15 cycles, but afterwards the reversible capacity drops rapidly, resulted in a quite lower capacity retention of 49.5% than that of $Co_2SnO_4/Co_3O_4/Al_2O_3/C$ (77.8%). This strongly suggests the necessary buffering effect of non-active Al_2O_3. The buffering role can also be supported by comparing the Co_2SnO_4/Co_3O_4 and $Co_2SnO_4/Co_3O_4/Al_2O_3$ electrodes, *viz*. with and without Al_2O_3. Upon the 100th cycle, we found that low charge capacities are 388 and 459 mA h g^{-1} for Co_2SnO_4/Co_3O_4 and $Co_2SnO_4/Co_3O_4/Al_2O_3$, respectively. This appreciable difference clearly reveals that the $Co_2SnO_4/Co_3O_4/Al_2O_3$ is indeed capable of delivering a slightly improved cycling performance owing to the buffering effect of non-active Al_2O_3. This inactive component strategy has also been applied to electrodes for LIBs, typically involving several-nanometer-thick ultrathin coating of Al_2O_3 on $LiCoO_2$ achieved by expensive ALD technique[51] or exquisite control pH value of buffer solution,[52] Al_2O_3 matrix to support Cu_2Sb-Al_2O_3-C composite synthesized via a high-energy mechanical reduction of Sb_2O_3 with Al and Cu metals in the presence of carbon (acetylene black).[53] In our case, considering the unique flexibility of varying type and stoichiometric ratio of LDH cations over a wide range, the LDH precursor-derived preparation method could be relatively simple and suitable to produce large quantities of multi-component nanomaterials for practical application.

On the other hand, we can see from Fig. 5c that both electrodes ($Co_2SnO_4/Co_3O_4/Al_2O_3/C$ and $Co_2SnO_4/Co_3O_4/C$) with carbon indeed exhibit highly enhanced reversible capacities and cycling stabilities, compared with the other two ones ($Co_2SnO_4/Co_3O_4/Al_2O_3$ and Co_2SnO_4/Co_3O_4) without carbon, respectively. Obviously, the supporting carbon play a critical role in boosting conductivity and further electrochemical performances, as well-recognized by various previous studies of carbon-supported anode nanomaterials.[54,55]

Rate capability was examined for the $Co_2SnO_4/Co_3O_4/Al_2O_3/C$ electrode and those three electrodes for comparison. Fig. 5d shows that the $Co_2SnO_4/Co_3O_4/Al_2O_3/C$ electrode exhibits the reversible capacities of 1420, 1285, 1110, 920, 770, and 584 mA h g^{-1} at the current densities of 100, 200, 400, 800, 1000, and 2000 mA g^{-1}. The reversible specific capacity was found to return to 1245 mA h g^{-1} when the current density was 100 mA g^{-1}, suggesting that the $Co_2SnO_4/Co_3O_4/Al_2O_3/C$ electrode remains very stable during cycling. However, the other three electrodes indeed exhibit much lower rate capacities at the other corresponding current densities in comparison with the $Co_2SnO_4/Co_3O_4/Al_2O_3/C$ electrode. On the basis of the distinctly enhanced electrochemical performances of $Co_2SnO_4/Co_3O_4/Al_2O_3/C$ among all the composite electrodes, we thus believe that the high enhancements of the $Co_2SnO_4/Co_3O_4/Al_2O_3/C$ electrode benefit from the multiple component synergistic contributions: (i) combined conversion and alloying reactions of nanosized bi-active Co_2SnO_4/Co_3O_4 during cycling; (ii) buffering Al_2O_3 and carbon, which are well-known to accommodate strain change and prevent aggregation of active components; and (iii) conductive carbon to improve the conductivity of the electrode and thereby rapid electronic transport.

Electrochemical impedance spectra (EIS) were reordered for those four electrodes to support the improved conductivity.

Figure 6 shows that the impedance spectra consists of a high-to-medium-frequency depressed semicircle and a low-frequency sloping linear line. Basically, the high frequency semicircle is attributed to SEI resistance and contact resistance, the medium-frequency semicircle is assigned to the charge-transfer impedance of the electrode reaction at the electrode/electrolyte interface, and the low-frequency sloping linear tail corresponds to the Warburg impedance that reflects solid-state diffusion of lithium ions within the bulk electrode.[56-59] The impedance spectra of the electrodes with carbon both exhibit smaller semicircle diameters compared with those without carbon. The values of semicircle diameters of the $Co_2SnO_4/Co_3O_4/Al_2O_3/C$ and $Co_2SnO_4/Co_3O_4/C$ composites were determined to be 36.9 and 36.7 Ω, respectively, much lower than those of Co_2SnO_4/Co_3O_4 and $Co_2SnO_4/Co_3O_4/Al_2O_3$ (60.9 and 86.3 Ω, respectively). In addition, it is noteworthy that both electrodes with carbon show smaller Warburg impedances when compared with

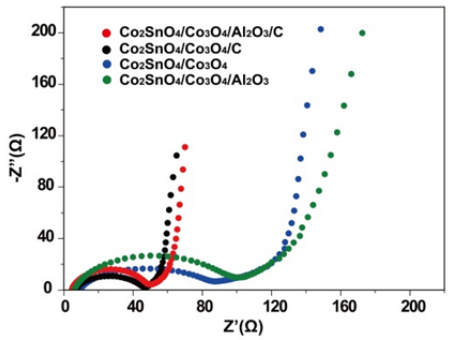

Fig. 6 Comparison of Nyquist plots for the electrodes of $Co_2SnO_4/Co_3O_4/Al_2O_3/C$, Co_2SnO_4/Co_3O_4, $Co_2SnO_4/Co_3O_4/Al_2O_3$ and $Co_2SnO_4/Co_3O_4/C$.

those without carbon. These decreases clearly suggest that the electrodes with carbon are able to possess the improved electrical conductivity and deliver an enhancement effect in the kinetics for lithium storage. Although the $Co_2SnO_4/Co_3O_4/Al_2O_3/C$ electrode contains the low-mass-weight non-active Al_2O_3, the electrode is able to exhibit a low impedance quite close to that of the $Co_2SnO_4/Co_3O_4/C$ electrode, and eventually deliver the highly improved electrochemical performances, as a result of synergistic contributions from the conductive carbon, bi- and non-active components.

4 Conclusions

We have demonstrated an easy method to prepare multi-component $Co_2SnO_4/Co_3O_4/Al_2O_3/C$ composite as efficient anode nanomaterials for LIBs. The $Co_2SnO_4/Co_3O_4/Al_2O_3/C$ electrode is able to exhibit a highly enhanced reversible capacity of 1170 mA h g^{-1} upon 100 cycles, compared with the designed bi-active Co_2SnO_4/Co_3O_4 composites without Al_2O_3 or carbon ($Co_2SnO_4/Co_3O_4/C$, $Co_2SnO_4/Co_3O_4/Al_2O_3$, and Co_2SnO_4/Co_3O_4) prepared by tuning cation types of LDH precursors through the same protocol. The componential and nanostructural features are capable of facilitating the reversible capacity contributed from synergistic effect of bi-active Co_2SnO_4/Co_3O_4 and multi-electron reaction during the cycle processes, and also the high cycling and rate stabilities from the buffering role of non-active Al_2O_3 and carbon, as well as the improved conductivity of the carbon matrix. Our LDH precursor based approach may be extended to prepare other carbon-supported metal oxides as lithium-storage hybrid nanomaterials, on the basis of the great versatility in varying the metal cations and surfactant interlayer anions of LDH precursors.

Acknowledgements

This work was supported by National Basic Research Program of China (973 Program 2014CB932102) and National Natural Science Foundation of China, as well as and the Program for Changjiang Scholars and Innovative Research Team in University (IRT1205).

Notes and references

1 D. Larcher and J. M. Tarascon, *Nat. Comm.,* 2015, **7**, 19.
2 H. Sun, G. Xin, T. Hu, M. Yu, X. Sun, J. Lian and D. Shao, *Nat. Comm.,* 2014, **5**, 4526.
3 Y. Q. Fu, X. Y. Wang, H. Wang, Y. W. Zhang, X. K. Yang, H. B. Shu, *RSC Adv.*, 2015, **5**, 14531.
4 Y. Zhang, W. Zhang, Z. Yang, H. Gu, Q. Zhu, S. Yang and M. Li, *Angew. Chem. Int. Ed.,* 2015. **54**, 3932.
5 J. Wang, B. Gao, L. Zhang, R. Li, J. P. Shen, Z. Q. Qiao, G. C. Yang, F. D. Nie, RSC Adv., 2015, 4, 14531.
6 H. Guo, T. Li, W. Chen, L. Liu, X. Yang, Y. Wang and Y. Guo, *Nanoscale,* 2014, **6**, 15168.
7 J. Zhang, J. Liang, Y. Zhu, D. Wei, L. Fan and Y. Qian, *J. Mater. Chem. A,* 2014, **2**, 2728.
8 W. Kang, Y. Tang, W. Li, X. Yang, H. Xue, Q. Yang, and C. S. Lee, *Nanoscale*, 2015, **7**, 225.
9 M. Li, C. Li, F. Zhang, L. J. Wan, S. Xu and D. G. Evans, *Chem. Comm.,* 2012, **48**, 410.
10 D. Wang, X. Chen, D. G. Evans and W. Yang, *Nanoscale,* 2013, **5**, 5312.
11 R. Zhang, Y. He, A. Li and L. Xu, *Nanoscale,* 2014, **6**, 14221.
12 J. Cabana, L. M. D. Larcher and M. R. Palacin, *Adv.Mater.,* 2012, **22**, E170.
13 D. Zhao, Y. Xiao, X. Wang, Q. Gao and M. Cao, *Nano Energy,* 2014, **7**, 124.
14 Y. Idota, *Science,* 1997, **276**, 1395.
15 X. Meng, X. Q. Yang and X. Sun, *Adv. Mater.,* 2012, **24**, 3589.
16 L. Hou, L. Lian, L. Zhang, G. Pang, C. Yuan and X. Zhang, *Adv. Func. Mater.,* 2015, **25**, 238.
17 G. Li, Y. Wang, L. Yang, W. Ma and M. Wang, *Eur. J. Inorg. Chem.,* 2014, **5**, 845.
18 Q. H. Wu, B. Qu, J. Tang, C. Wang, D. Wang, Y. Li and J. G. Ren, *Electrochim. Acta,* 2015, **156**, 147.
19 J. S. Luo, M. T. Mayer, M. Schreier, M. K. Nazeeruddin, S. D. Tilley, H. J. Fan and M. Grätzel, *Science,* 2014, **345**, 1593.
20 P. Tang, Y. Feng, D. Li, *Dyes Pigments,* 2014, **104**, 131.
21 Z. Sun, L. Jin, W. Shi, M. Wei, D. G. Evans and X. Duan, *Langmuir,* 2011, **27**, 7113.
22 R. Huo, Y. Kuang, Z. Zhao, F. Zhang and S. Xu, *J. Coll. and Interf. Sci.,* 2013, **407**, 17.
23 Z. Liang, R. Huo, Y. X. Yin, F. Zhang, S. Xu and Y. G. Guo, *Electrochim. Acta,* 2013, **108**, 429.

24 B. An, Q. Ru, S. Hu, X. Song and J. Li, *Mater. Res. Bull.,* 2014, **60**, 640.
25 H. Hu, B. Guan, B. Xia and X. W. Lou, *J. Am. Chem. Soc.,* 2015, **137**, 5590-5596.
26 Y. Qi, N. Du, H. Zhang, P. Wu and D. Yang, *J. Power Sources,* 2011, **196**, 10234.
27 S. D. Li, J. Lu, M. Wei, D. G. Evans and X. Duan, *Adv. Funct. Mater.,*2010, **20**, 2848.
28 Z. Liang, R.Huo, S. Yin, F. Zhang and S. Xu, *J. Mater. Chem. A,* 2014, **2**, 921.
29 J. P. Liu, Y. Y. Li, X. T. Huang, G. Y. Li, Z. K. Li, *Adv. Funct. Mater.*, 2008, **18**, 1448.
30 H. Yang, *J. Phys. Chem. B,* 2007, **111**, 8006.
31 S. Yuvaraj, S. Amaresh, Y. S. Lee and R. K. Selvan, *RSC Adv.,* 2014, **4**, 6407.
32 S. Ikeda, Y. H. Ng, Y. Ikoma, T. Sakata, H. Mori, T. Harada and M. Matsumura, *Chem. Mater.,* 2007, **19**, 4335.
33 L. Xu, Y. Ding, Y. Peng, S. Zhang, W. Yu and Y. Qian, *J. Phys. Chem. B,* 2004, **108**, 10859.
34 D. Bresser, R. Kloepsch, S. Krueger, M. Fielder, R. Schmitz, D. Baither, M. Winter and S. Passerini, *Adv. Energy Mater.,* 2013, **3**, 513.
35 C. He, N. Zhao, C. Shi, E. Liu and J. Li, *ACS Nano,* 2013, **7**, 4459.
36 F. Li, S. L. X., Y. R. Liu, Z. C. Ju and Y. T. Qian, *ACS Appl. Mater. Interface,* 2013, **5**, 981.
37 C. Chen, Q. Ru, S. Hu, B. An, X. Song and X. Hou, *Electrochim. Acta,* 2015, **151**, 203.
38 S. Xiong, J. S. Chen, X. W. Lou, H. C. Zeng, *Adv. Funct. Mater.,* 2012, **22**, 861.
39 B. S. Umansky and E. A. Lombardo, *Appl. Catal.,* 1987, **31**, 275.
40 H. Qiao, L. F. Xiao, Z. Zheng, H. W. Liu, F. L. Jia and L. Z. Zhang, *J. Power Sources*, 2008, **185**, 486.
41 X. X. Zhang, Q. S. Xie, G. H. Yue, Y. Zhang, X. Q. Zhang, A. L. Lu and D. L. Peng, *Electrochim. Acta,* 2013, **111**, 746.
42 G. Wang, X. P. Gao and P. W. Shen, *J. Power Sources,* 2009, **192**, 719.
43 P. Poizot, S. Grugeon, L. Dupont, J. M. Tarascon, *Nature*, 2000, **407**, 496.
44 P. J. Sideris, U. G. Nielsen, Z. Gan, C. P. Grey, *Science*, 2008, **321**, 113.
45 J. Liang, X. Yu, H. Zhou, H. B. Wu, S. J. Ding and X. W. Lou, *Angew. Chem. Int. Ed.,* 2014, **53**, 1.
46 J. S. Cho, Y. J. Hong and Y. C. Kang, *ACS Nano*, 2015, **9**, 4026.
47 J. Y. Wang, N. L. Yang, H. J. Tang, Z. H. Dong, Q. Jin, M. Yang and D. Wang, *Angew. Chem. Int. Ed.*, 2013, **125**, 6545-6548.
48 J. Sun, H. M. Liu, X. Chen, D. G. Evans and W. S. Yang, *Nanoscale*, 2013, **5**, 7564.
49 Y. S. Luo, D. Z. Kong, J. S. Luo, Y. L. Wang, D. Y. Zhang, K. W. Qiu, C. W. Cheng, C. M. Lid, T. Yu, *RSC Adv*., 2014, **4**, 13241.
50 W. S. Kim, Y. Hwa, H. C. Kim, J. H. Choi, H. J. Sohn and S. Hong, *Nano Res.,* 2014, **7**, 1128.
51 I. D. Scott, Y. S. Jung, A. S. Cavanagh, Y. Yan, A. C. Dillon, S. M. George and S. H. Lee, *Nano Lett.,* 2011, **11**, 414.
52 W. Zhang, Z. X. Chi, W. X. Mao, R. W. Lv, A. M. Cao and L. J. Wan, *Angew. Chem. In. Ed.,* 2014, **53**, 12776.
53 D. Applestone, S. Yoon and A. Manthiram, *J. Mater. Chem.*, 2012, **22**, 3242.
54 L. Zhang, H. B. Wu, B. Liu and X. W. Lou, *Energy Enviro. Sci.,* 2014, **7**, 1013.
55 F. Han, W. C. Li, C. Lei, B. He, K. Oshida and A. H. Lu, *Small,* 2014, **10**, 2637.
56 J. W. Zhou, J. Qin, X. Zhang, C. S. Shi, E. Z. Liu, J. J. Li, N. Q. Zhao, C. N. He, *ACS Nano*, 2015, **9**, 3837.
57 S. H. Choi, Y. N. Ko, J. K. Lee, Y. C. Kang, *Adv. Funct. Mater.*, 2015, **25**, 1780.
58 T. Hang, D. Mukoyama, H. Nara, T. Yokoshima, T. Momma, M Li, T. Osaka, *J. Power Sources*, 2014, **256**, 226.
59 O. S. M. Hernandez, H. Ishikawa, Y. Nishikawa, Y. Maruyama, Y. Sone, Mi. Umeda, *Electrochim. Acta*, 2014, **131**, 168.

Graphical abstract

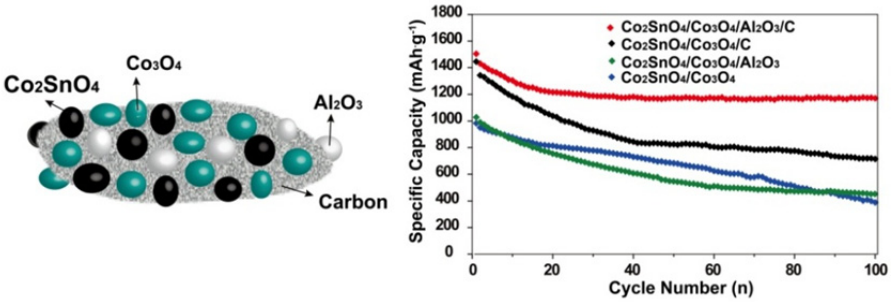

$Co_2SnO_4/Co_3O_4/Al_2O_3/C$ composite is prepared from a laurate anion-intercalated CoAlSn-layered double hydroxide single-source precursor, and delivers highly enhanced electrochemical performances.